

Simulation and performance Analysis of a Novel Model for Short Range Underwater Acoustic communication Channel Using Ray Tracing Method in Turbulent Shallow Water Regions of the Persian Gulf

Mohammad Javad Dargahi , Abdollah Doosti Aref , Dr Ahmad Khademzade

Islamic Azad university ; Central Tehran Branch
Department of electrical engineering

Abstract

High data rate acoustic transmission is required for diverse underwater operations such as the retrieval of large amounts of data from bottom packages and real time transmission of signals from underwater sensors. The major obstacle to underwater acoustic communication is the interference of multipath signals due to surface and bottom reflections. High speed acoustic transmission over a shallow water channel characterized by small grazing angles presents formidable difficulties. The reflection losses associated with such small angles are low, causing large amplitudes in multi-path signals. In this paper, based on the results obtained from practical measurements in the Persian Gulf and available data about sound speed variations in different depths, we propose a simple but effective model for shallow water short-range multipath acoustic channel. Based on the Ray theory, mathematical modeling of multipath effects is carried out. Also in channel modeling, the attenuation due to the wave scatterings at the surface and its bottom reflections for deferent grazing angles and bottom types is considered. In addition, we consider the attenuations due to the absorption of different materials and ambient noises such as sea-state noise, shipping noise, thermal noise and turbulences. We use a three-dimensional hydrodynamic model (COHERENS) in a fully prognostic mode to study the

circulation and water mass properties of the Persian Gulf – a large inverse estuary. Maximum sound speed occurs during the summer in the Persian Gulf which decreases gradually moving from the Strait of Hormuz to the north western part of the Gulf. A gradual decrease in sound speed profiles with depth was commonly observed in almost all parts of the Gulf. However, an exception occurred in the Strait of Hormuz during the winter. The results of the model are in very good agreement with our observations.

Keywords: Persian Gulf , shallow water , acoustic channel , Ray theory.

1- Introduction

High data rate acoustic transmission is required for diverse underwater operations such as the retrieval of large amounts of data from bottom packages and real time transmission of signals from underwater sensors. However, acoustic signals transmitted in shallow water are corrupted by interference from reflection and scattering at the water surface and bottom. For this reason, the shallow underwater channel is a difficult medium in which to achieve the high data rates needed for many applications. An especially difficult

problem is that the acoustic signal transmitted over a shallow water channel has associated with it inherently small grazing angles and small reflection losses. This results in significant corruption due to large amplitude multi-path signals [1], [2]. Therefore, it is very important to construct a good model of the channel and design a satisfactory communication system for this environment. This paper introduces a model that describes a shallow underwater channel using geometric and environmental parameters.

The model utilizes the impulse response of the channel with weighting according to the attenuation due to reflection, absorption etc., and windowing techniques to determine the signal-to-corruptive multi-path signal ratio (SMR) in the observation window [3], [4].

In the deep ocean multi-path signals are attenuated by spreading and reflection losses at relatively large grazing angles. The effects of this multi-path interference can be reduced by using a directional transmitter and/or receiver. However, spatial discrimination of direct path and multi-path signals by directional arrays in shallow water is virtually impossible. On the other hand, under certain conditions the primary multi-path signals can add constructively to increase the strength of the received signal. This indicates that a high rate, coherent communication is possible for a wide range of channel geometries and parameters. We show the relationship between the achievable error-free transmission rate and the SMR. The results of computer analysis indicate that transmission rates in excess of 8 k-bits/s are possible over a distance of 13 km

and in a water depth of only 20 meters using the phase-shift-keying system (PSK).

Sea water acts as an acoustic waveguide and transmits sound signal in itself. Sound channel as a sound waveguide is a channel with random parameters. But this subject does not have the meaning of its unpredictability. The most important characteristic of sea water is its inhomogeneous nature. In the whole classifications, its inhomogeneity can be classified into two regular and random groups. Regular variations of sound speed in different layers of water leads to the formation of sound channel and this phenomenon causes the long distance sound propagation. Random homogeneity causes the scattering of sound waves and sound fields variation. Hence, in this section, as an introduction, viewpoint and basic step, investigate the variation of sound speed profile in the Persian Gulf. The Persian Gulf, referred to in some local countries as the Arabian Gulf, is an important military, economic and political region owing to its oil and gas resources and is one of the busiest waterways in the world. Countries bordering the Persian Gulf are the United Arab Emirates, Saudi Arabia, Qatar, Bahrain, Kuwait and Iraq on one side and Iran on the other side (Fig. 1). The Persian Gulf is a semi-enclosed, marginal sea that is exposed to arid, sub-tropical climate. It is located between latitudes 24°–30° N, and is surrounded by most of the Earth's deserts. The most known weather phenomenon in the Persian Gulf is the Shamal, a northwesterly wind which occurs year round [5]. In winter, the Shamal is of intermittent nature associated with the passage of synoptic weather systems, but it seldom exceeds a speed of 10 m/s. The summer Shamal is

of continuous nature from early June through to July. Seasonal variations of the Shamal are associated with the relative strengths of the Indian and Arabian thermal lows [6]. Tectonic driven subsidence deepened the seafloor of the Strait on its southern side (200–300m depths are seen in some localized seafloor depressions) and produced a 70–95m deep trough along the Iranian side of the eastern part of the Gulf. A southward widening channel leads from the Strait south across a series of sills (water depth of ~110 m) and shallow basins to the shelf edge [7]. The narrow Strait of Hormuz restricts water exchange between the Persian Gulf with the northern Indian Ocean [8].

southern part of the Gulf except of the region surrounding Bahrain, it varies from 1548-1552 m/s at the bottom layer and from 1553-1557 m/s at the surface layer. These regions are shallow (up to 100 m) and the difference between surface and bottom temperature is negligible, therefore, sound speed is a function of both temperature and salinity [9]. Besides, Around Bahrain, it varies from 1539-1544 m/s at the bottom and from 1554-1558 m/s at the surface. In this part of the gulf, sound speed varies more than other parts because this region is shallow and salinity has more effects than temperature on sound speed [10],[11]. In the neighborhood of Iraq and Kuwait, due to the salinity of the water, the sound speed at the bottom is more than the surface. It can be obviously seen that, from the Strait of Hormuz to the western regions of the Persian Gulf, the sound speed versus the depth is reduced.

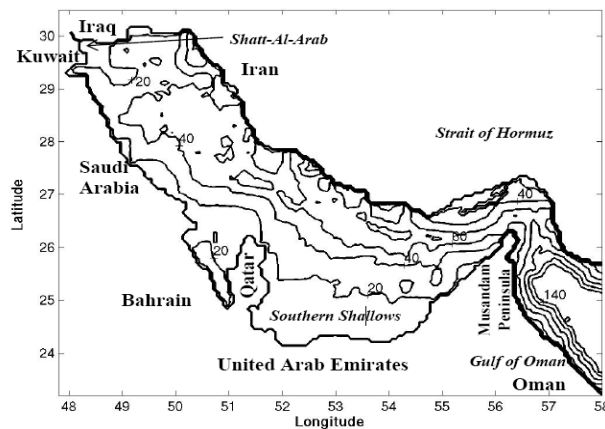


Fig.1: Bathymetry used in this study

According to the obtained measurements, as can be shown from fig. 2, sound speed is maximum during the summer (~1560 m/s) in the southern part of the Persian Gulf [9]. Also sound speed in the northern part of the Gulf varies from 1524-1528 m/s at the bottom and from 1547-1552 m/s at the surface [5]. These show that it has a 20 m/s difference from surface to bottom. In the

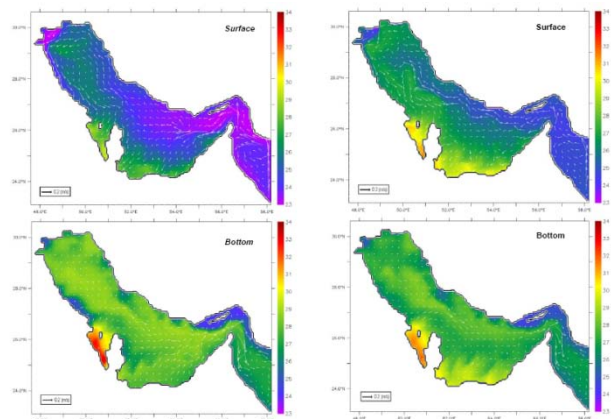


Fig.2: Sound speed (from 1500 m/s) in surface and bottom layers in different parts of the Persian Gulf [9]

2- Modification of Medwin formula in order to adapting with the measured data in The Persian Gulf.

In this section, based on the performed measurements [12], to adapt the output of Medwin's equation [13] with the measured sound speed profile in the Persian Gulf, Medwin equation is modified. In Fig.4, profile of the sound speed variations versus depth in the Strait of Hormoz is shown on 56.7E° and 25.4N°, in conditions that water depth was 85m and the ADCP measurement tool, belonged to the NOAA submarine on Aug, 2, 2007, placed at the depth of 10m. By considering the subject of fix variation of sound speed versus temperature and salinity in shallow waters, which is between 1500 to 1502 m/s, the horizontal axis of this figure shows the difference of the measured sound speed with 1500 m/s. Also, the vertical axis of the profile depicts depth variations.

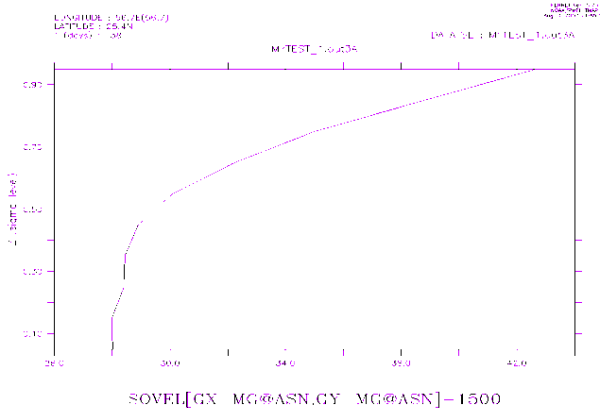


Fig.3: Sound speed profile of the Persian Gulf [12]

The relation of sound speed variations versus salinity and temperature in Medwin's formula is given in Eq. (1) [13]. According to the salinity and measured temperature from practical experiments for the profile of Fig. 3, the

obtained results (temperature=33.56°C, salinity=38.37 ppt) from Eq. (1) are in the range of 1500 to 1501 (m/s) actually.

$$C = 1449.2 + 4.6T + 0.055T^2 + 0.00029T^3 + (1.34 - 0.01T)(S - 35) \quad (1)$$

Eq. (2) is the modified version of Medwin formula that we have presented. In this equation, dependence of sound speed to the salinity and temperature is adapted with the Medwin formula. However, in this case, the sound variations versus depth is approximated by a 10th order polynomial [8].

$$C = 1449.2 + 4.6T + 0.055T^2 + 0.00029T^3 + (1.34 - 0.01T)(S - 35) - 8.28 \times 10^{-6} D^{10} - 0.0024 D^9 + 0.31 D^8 - 0.24 D^7 + 1.2 \times 10^{-3} D^6 - 4.2 \times 10^{-4} D^5 + 10^{-6} D^4 - 1.6 \times 10^{-7} D^3 + 1.1 \times 10^{-9} D + 3.1 \times 10^{-9} \quad (2)$$

Fig. 4 illustrates the output of the Medwin formula, the output of the obtained modified formula, and the experimental data. In this figure, the approximation error (3%) for each point is well acceptable.

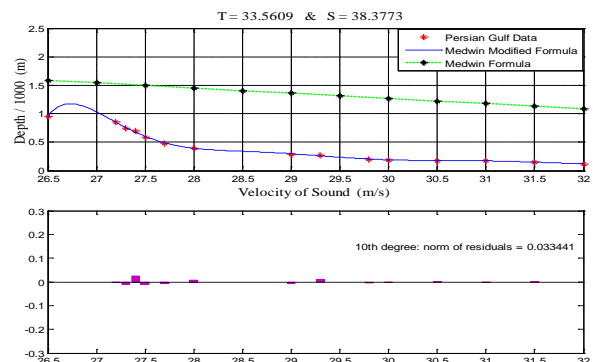


Fig.4: Obtained profile from Medwin's formula, Medwin's modified formula and measured data. The difference between real data and the presented model

3- Channel modeling

In channel modeling, the attenuations due to the frequency absorption, ambient noises and loss due to the wave scatterings at the surface and bottom for deferent grazing angles and bottom types are considered. Also, Ray theory is the basis of the mathematical model of multipath effects.

3-1- loss modeling

The acoustic energy of a sound wave propagating in the ocean is partly:

- Absorbed, i.e. the energy is transformed into heat.
- lost due to sound scattering by inhomogeneities.

On the basis of extensive laboratory and field experiments [13], the attenuation due to the absorption effects of Boric acid, $B(OH)_3$, Magnesium sulphate, $MgSO_4$ and pure water, H_2O is considered. The total loss is the sum of the each material loss. Experimental measurements and obtained profile for each material and the total loss are shown in Fig 5.

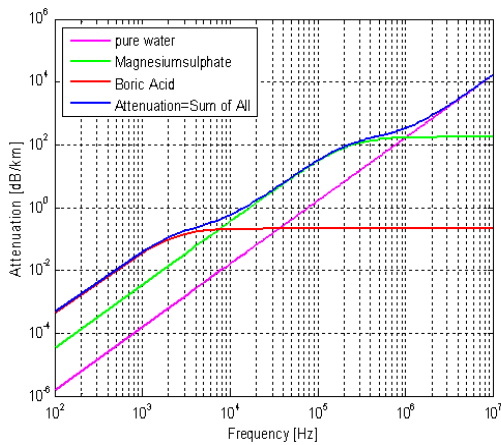


Fig.5: Amount of measured loss in different frequencies

From Fig. 5, it can be observed that for the *Boric acid* region, Attenuation is proportional to f^2 . And for the regions

Magnesium sulphate and pure water also Attenuation is proportional to f^2 . In the transition domains it is proportional to f . Attenuation increases with increasing salinity and temperature, Fig. 6. Attenuation increases with increasing frequency.

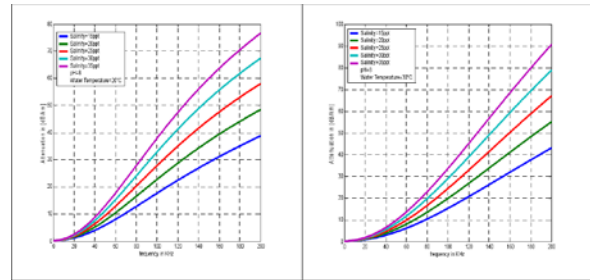


Fig. 6: Attenuation plot for various salinities & for temperature a) 20°C b) 30°C

3-2- Noise modeling

The model considered for noise is the combination of the thermal noise, shipping noise sea state noise and turbulences [14]. Eq. (3) depicts the general relation of the ambient noise:

$$(3) \quad NL = 10 \log_{10} \left(10^{0.1NL_{traffic}} + 10^{0.1NL_{turbulence}} + 10^{0.1NL_{sea-state}} + 10^{0.1NL_{thermal}} \right)$$

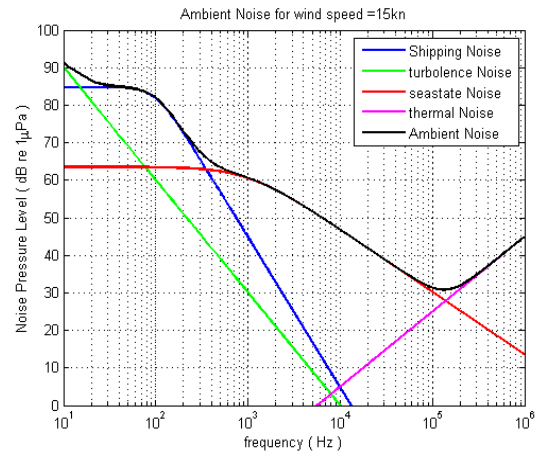


Fig. 7: Ambient noise Level for deferent frequency domains [4]

3-3- Scattering modeling in the surface and bottom reflections

To calculate loss due to the wave scattering in the surface, we use the probably density function of Gaussian Normal distribution for the surface displacement variable.

In the simulation, average of the reflection coefficient is calculated from Eq. (4) [15]:

$$R_{Gauss} = Re^{-2(kh)^2 \cos^2 \phi} \quad (4)$$

Where k denotes the wave number, h is the effective value of the surface wave height, ϕ is the angle of the collision to the normal surface, R is the pressure reflection for the normal surface. We consider $R=-1$ and h is obtained from the spectral density of the water surface displacement. The most famous spectrum in this case is Neumann-Pierson spectrum. For the calculation of wave bottom reflection coefficient, we use the Jackson pattern to select bottom water type which is simulated based on the Strait of Hormoz conditions and Hamilton-Bachman model [15],[16].

From Fig. 8, it can be observed that with an increase of grazing angle the scattering loss also increases. In the same way with the increase of wind speed, there is an increase in scattering loss. Similarly we can also observe the dependence of Bottom reflection coefficient, on grazing angle ϕ_m and bottom type bt . This is illustrated in Fig. 9.

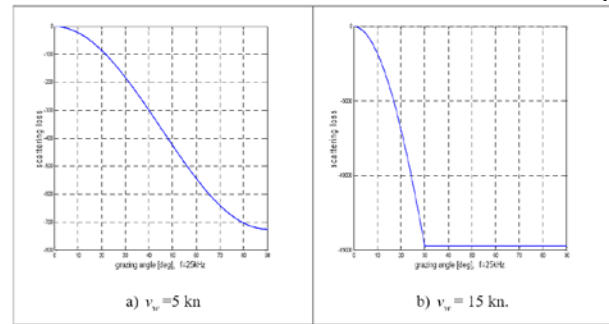


Fig. 8: Diagram illustrating dependence of surface reflection coefficient on grazing angle, frequency and two wind speeds

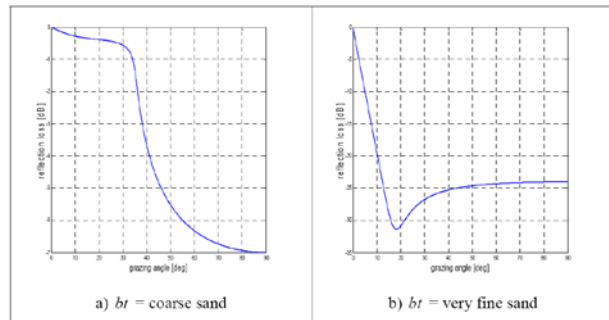


Fig. 9: Diagram illustrating dependence of bottom reflection coefficient on grazing angle and two bottom types

3-4- Modeling of Multipath

In the performed simulation, the number of the channel paths is varied and multiple of four. In the considered model, for the wave propagation from transmitter to receiver, we use four rays (Eigen rays). The transmitted wave is either one of the four Eigen rays or the multiple of them.

In the second case, after several reflections, the wave is reached to the receiver in one of the four cases shown in Fig.8. In the image method, according to Fig.9, surface and bottom are considered as the two mirrors. In the cylindrical coordinates for the channel with depth of D , surface is at $Z=0$ and bottom is at $Z=D$ [12]. Assume that transmitter is at $(0, Z_s)$ and receiver is at $(0, Z_r)$. Therefore, the first image of transmitter which is due to the mirror

effect of the surface, is located in $(0, -Z_s)$. Then transmitter and this image in relation to the bottom are located at $(0, 2D - Z_s)$ and $(0, 2D + Z_s)$ and making the second and third images, respectively. In general case, number of images or the sources of virtual transmitter equal to infinity and in each of the image repeating, four new images are generated that each of them are related to one of the eigen rays. According to this theory, the field of the pressure sound is depicted with Eq. (5) [15],[16].

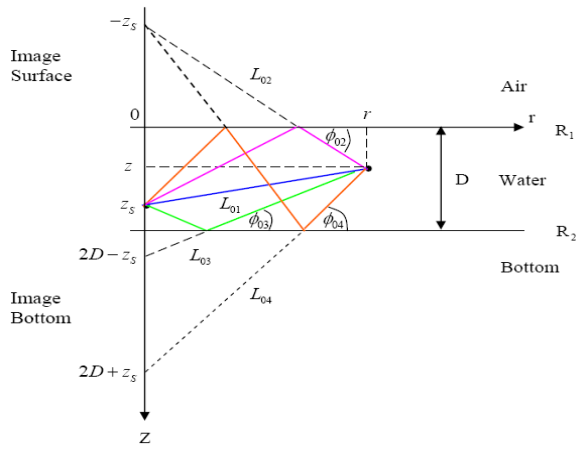


Fig.10: Schematic of transmitter and first three images in the image theory for a Homogenous channel

$$P(r, z, \omega) = A(\omega) \sum_{m=0}^{\infty} \left\{ \begin{aligned} & \hat{R}_1^m(\varphi_{m_1}, \omega) \hat{R}_2^m(\varphi_{m_1}, \omega) \frac{e^{-jkL_{m_1}}}{L_{m_1}} \\ & + \hat{R}_1^{m+1}(\varphi_{m_2}, \omega) \hat{R}_2^m(\varphi_{m_2}, \omega) \frac{e^{-jkL_{m_2}}}{L_{m_2}} \\ & + \hat{R}_1^m(\varphi_{m_3}, \omega) \hat{R}_2^{m+1}(\varphi_{m_3}, \omega) \frac{e^{-jkL_{m_3}}}{L_{m_3}} \\ & + \hat{R}_1^{m+1}(\varphi_{m_4}, \omega) \hat{R}_2^{m+1}(\varphi_{m_4}, \omega) \frac{e^{-jkL_{m_4}}}{L_{m_4}} \end{aligned} \right\} \quad (5)$$

In this equation, A is the amplitude of the sound wave, R_1, R_2 are the reflection

coefficients of the surface and bottom respectively. $\phi_{m1}, \dots, \phi_{m4}$ are the reflection angles of the four eigen rays, K is the wave number and $L_{m1}, L_{m2}, L_{m3}, L_{m4}$ are the length of the displacement vectors of eigen rays RSRBR, RBR, RSR, DP in the $(m+1)^{th}$ stage of the production cycle of virtual resources, respectively. By considering the location of generated image in the m^{th} stage, the displacement vectors length of propagation paths are in accordance with Eq. (6) [15],[16].

$$\begin{aligned} L_{m_1} &= \sqrt{r^2 + (2Dm - z_s + z)^2} \\ L_{m_2} &= \sqrt{r^2 + (2Dm + z_s + z)^2} \\ L_{m_3} &= \sqrt{r^2 + (2D(m+1) - z_s - z)^2} \\ L_{m_4} &= \sqrt{r^2 + (2D(m+1) + z_s - z)^2} \end{aligned} \quad (6)$$

In the performed simulation, each of the reflection coefficients of the surface or bottom is calculated based on the introduced pattern of section. For Persian Gulf channel with considering $m=1$, i.e. eight paths, we concluded that from sixth path, due to the strong attenuation of transmitted wave, there is no signal reception. Hence, five-path channel pattern is suitable for the Persian Gulf.

4- Simulation

In this section, the obtained results for the channel, which its speed profile was shown in Fig.4, in conditions that channel depth was 5m and range of 1Km is presented. In this case, the transmitter and receiver use QPSK modulation with bandwidth of 5KHz and carrier frequency of 27KHz. Also, the transmitter and receiver are at depth of 5m and 70m from the surface, respectively. In Fig.11, the power spectral density of the transmitted signal

in the channel for each of the special paths is shown. As expected, in the RSRBR path, the largest attenuation takes place and power level in this path in comparison with direct path has 23dB loss. Also, received waves in the output of the channel in each of the 8 paths are shown in Fig.12. It can be seen that for sixth path and other paths after it, signal is strongly attenuated.

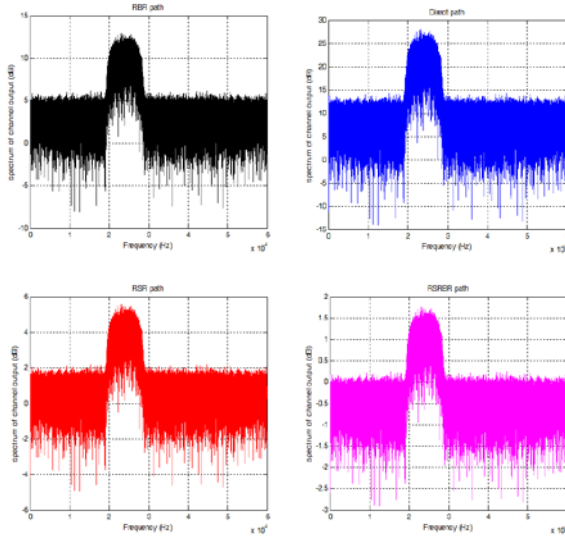


Fig. 11: Power spectrum density of the four special paths used in the simulation

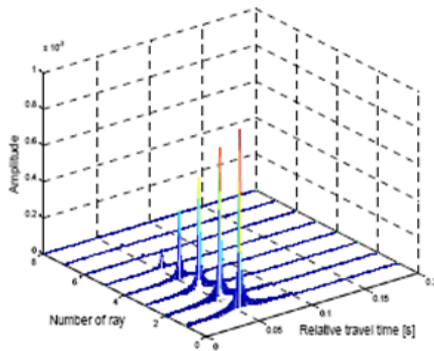


Fig. 12: Received signals from different paths of channel. In this model, channel has 8 paths. First signal is for the direct path and the delays of other paths are calculated based on the traveling time of the first path.

Conclusion

Findings presented in this paper and summarized in the following provide new insight into a novel model for shallow water short-range multipath acoustic channel in the Persian Gulf. Our results, which are in good agreement with the results obtained from field measurement in the Strait of Hormuz, suggest the following.

Based on the simulations carried out in this paper, in the first place, the densest water in the Persian Gulf forms during winter in shallow waters along the coast of United Arab Emirates (Southern Shallows) and around Bahrain. This is associated with atmospheric cooling of extremely saline water masses in shallow water. Overall, the evaporative salinity increase throughout the Gulf leads to a steady component of dense water outflow through the Strait of Hormuz. In summer and autumn, the bottom outflow extends the entire length of the Gulf. Secondly we present Eq. (2) as a suitable empirical formula which describes the sound speed profile in the Strait of Hormuz. In addition, in accordance with the patterns introduced in sections 1 to 4, considering the five-path channel model is proper for the mentioned region. To further improve understanding of the circulation including seasonal variations in the Persian Gulf, more field observations are required to close data gaps that exist for autumn months for the entire Gulf and year-round for the Southern Shallows. Also required is a better knowledge of current river discharge rates of the Shatt-al-Arab.

Future theoretical studies should investigate effects of both varied river discharge and synoptic-scale wind and heat-flux forcing on the circulation in the Persian Gulf. The focus hereby should

be placed into investigation of 1) heat fluxes and dense water formation in the Southern Shallows and 2) atmospheric conditions that promote formation of a coastal jet along the Iranian coast in the northern Gulf, not adequately described in our model simulations, and how this interacts with the gulf-wide circulation.

References

- [1] R. J. Urick, Principles of Underwater Sound, 3d ed. New York: McGraw-Hill, 1983, p. 129.
- [2] R. Coates, Underwater Acoustic Systems. New York: Macmillan Education Ltd., 1990, pp. 26-28.
- [3] R. J. Urick, "Intensity summation of modes and images in shallow-water sound transmission," J. Acoust. Soc. Amer., vol. 46, no. 3, pp. 780-788, Apr. 1999.
- [4] A. Zielinski, R. Coates, L. Wang, and A. Saleh, "High rate shallow water acoustic communication," Oceans 93, vol. 111, pp. 432437.
- [5] Emery, K. O., Sediments and water of the Persian Gulf, AAPG Bull., 40, 2354-2383, 1956.
- [6] Seibold, E. and Ulrich, J.: Zur Bodengestalt des nordwestlichen Golfs von Oman. "Meteor" Forsch. Ergebnisses, Reihe C, 3, 1-14, 2005.
- [7] Reynolds, R. M.: Physical oceanography of the Gulf, Strait of Hormuz, and the Gulf of Oman – Results from the Mt Mitchell expedition, Mar. Pollution Bull., 27, 35-59, 2007.
- [8] Johns, W. E., Yao, F., Olson, D. B., Josey, S. A., Grist, J. P., and Smeed, D. A.: Observations of seasonal exchange through the Straits of Hormuz and the inferred freshwater budgets of the Persian Gulf, J. Geophys. Res., 108(C12), 3391, doi:10.1029/2003JC001881, 2007.
- [9] Swift, S. A. and Bower, A. S.: Formation and circulation of dense water in the Persian/Arabian Gulf, J. Geophys. Res., 108(C1), 3004, doi:10.1029/2002JC001360, 2003.
- [10] Sadrinasab, M. and Kampf, J.: Three-dimensional flushing times in the Persian Gulf, Geophys. Res. Letters, 31, L24301, doi:10.1029/2004GL020425, 2008.
- [11] M. Sadrinasab, K. Kenarkoobi, "Numerical Modelling of sound velocity profile in different layers in the Persian Gulf", Asian journal of applied sciences, 232- 239, 2009, ISSN 1996-3343. Knowledge Review, Malaysia 2009.
- [12] A. Doosti Aref: Survey underwater acoustic communication with design and simulation of an Underwater acoustic communication system in the Persian Gulf, MSc thesis, Malek-e Ashtar Industrial University, Tehran, Iran, 2010.
- [13] H. Medwin and C.S. Clay, "Fundamentals of Acoustical Oceanography", Academic Press, San Diego, pp. 220-228, 2000.
- [14] R.J. Urick, "Ambient Noise in the sea", Peninsula Publishing, P.O.Box 867, California 94023, third edition, pp. 155-205, 1984.
- [15] L.M. Brekhovskikh and Yu. P. Lysanov, "Fundamentals of Ocean Acoustics", second edition. Springer-Verlag, pp. 130-155, 1999.
- [16] K. C. Hegewisch, N. R. Cerruti and S. Tomsovic, "Ocean acoustic wave propagation and ray method correspondence: internal wave fine structure," The Journal of the Acoustical Society of America, Vol. 114, Issue 4, p.2428, Oct.2007.